University of Groningen

An improved volume-of-fluid method for wave impact problems

Kleefsman, K.M. Theresa; Fekken, Geert; Veldman, Arthur E.P.; Iwanowski, Bogdan

[Link to publication in University of Groningen/UMCG research database](#)

An Improved Volume-of-Fluid Method for Wave Impact Problems

K.M. Theresa Kleefsman, Geert Fekken, Arthur E.P. Veldman
Dept. of Mathematics and Computing Science, University of Groningen
Groningen, the Netherlands

Bogdan Iwanowski
FORCE Technoloy Norway AS
Oslo, Norway

ABSTRACT

In this paper, a calculation method for wave impact problems is presented. This method is based on the Navier-Stokes equations and uses an improved volume-of-fluid (VOF) method for the displacement of the free surface. Results are shown for a dambreak simulation for which experimental results are available for comparison. Also drop tests have been simulated with wedges and circular cylinders. The results are very promising for the further development of the method.

KEYWORDS: Wave loading; moving body; numerical simulation; Cartesian grid; volume-of-fluid.

INTRODUCTION

There is a great need for calculation methods for local phenomena of wave impact loading and loading from green water on the deck of a ship. Most of the existing methods are not capable of predicting the local loads. Part of the Joint Industry Project SafeFLOW, initiated in January 2001, is devoted to the development of a method which is able to predict local wave impact on floaters operating in the offshore industry.

The development of the method, called COMFLOW, has started in 1995 with the simulation of liquid-filled spacecraft, that are tumbling in space [Gerrits, 2001]. In this application where the surface tension is the driving force, a good handling of the free surface is crucial. The method has also been applied to blood flow through (elastic) arteries, where no free surface was present [Loots, 2003]. A rather new application was found in the maritime world where sloshing inside anti-roll tanks has been simulated. In 1999 a pilot study of the simulation of green water on the deck of an FPSO has been performed, to investigate if the method is capable of capturing the local flow details on the deck [Buchner, 1999]. Because of promising results, it was decided to move on in this direction in the SafeFLOW project.

The simulation of fluid flow in COMFLOW is based on the Navier-Stokes equations for an incompressible, viscous fluid. The equations are discretised using the finite volume method. For the displacement of the free surface the VOF method has been used adapted with a local height function which is essential for a good simulation of the free surface flow. To simulate wave impact in a robust and accurate way, a good choice of the discrete boundary conditions at the free surface turns out to be very important.

In this paper, the model used in COMFLOW is described. Results are shown of simulations for a dambreak with a box in the flow. This simulation can be seen as a model of the water flow on the deck of a ship due to green water. Also results have been shown of water entry of two-dimensional objects. Comparison with theory and experiments is available.

GOVERNING EQUATIONS

Flow of a homogeneous, incompressible, viscous fluid is described by the continuity equation and the Navier-Stokes equations. The continuity equation describes conservation of mass and the Navier-Stokes equations describe conservation of momentum. In conservative form, they are given by

$$\oint_{\partial V} \boldsymbol{u} \cdot \boldsymbol{n} dS = 0, \tag{1}$$

$$\int_V \frac{\partial \boldsymbol{u}}{\partial t} dV + \oint_{\partial V} \boldsymbol{u}\boldsymbol{u}^{\mathrm{T}} \cdot \boldsymbol{n} dS =$$
$$-\frac{1}{\rho} \oint_{\partial V} (p\boldsymbol{n} - \mu \nabla \boldsymbol{u} \cdot \boldsymbol{n}) dS + \int_V \boldsymbol{F} dV. \tag{2}$$

Here, ∂V is the boundary of volume V, $\boldsymbol{u} = (u, v, w)$ is the velocity vector in the three coordinate directions, $\boldsymbol{n}$ is the normal of volume V, ρ denotes the density, p is the pressure, ∇ is the gradient operator. Further μ denotes the dynamic viscosity and $\boldsymbol{F} = (F_x, F_y, F_z)$ is an external body force, for example gravity. In the case that moving rigid bodies are present in the domain V, the above equations still hold, with the additional condition that the fluid velocity at the boundary of the object is equal to the object velocity.

Boundary conditions

At the solid walls of the computational domain and at the objects inside the domain, a no-slip boundary condition is used. This condition is described by $\boldsymbol{u} = 0$ for fixed boundaries, and $\boldsymbol{u} = \boldsymbol{u}_b$ for moving objects with $\boldsymbol{u}_b$ the object velocity.

Some of the domain boundaries may let fluid flow in or out of the domain. Especially, when performing wave simulations, an inflow boundary is needed where the incoming wave is prescribed and at the opposite boundary a non-reflecting outflow condition should be used. In our method, the wave on the inflow boundary can be prescribed as a regular linear wave or a regular 5th order Stokes wave. Also a superposition of linear components can be used which results in an irregular wave. At the outflow boundary, a Sommerfeld condition is very appropriate in cases where a regular wave is used. In the case of an irregular wave or a much deformed regular wave (e.g. due to the presence of an object in the flow) a damping zone is added at the end of the domain.

Free surface

If the position of the free surface is given by $s(x,t) = 0$, the displacement of the free surface is described using the following equation

$$\frac{Ds}{Dt} = \frac{\partial s}{\partial t} + (u \cdot \nabla)s = 0. \tag{3}$$

At the free surface, boundary conditions are necessary for the pressure and the velocities. Continuity of normal and tangential stresses leads to the equations

$$-p + 2\mu\frac{\partial u_n}{\partial n} = -p_0 + 2\gamma H \tag{4}$$

$$\mu\left(\frac{\partial u_n}{\partial t} + \frac{\partial u_t}{\partial n}\right) = 0. \tag{5}$$

Here, u_n is the normal component of the velocity, p_0 is the atmospheric pressure, γ is the surface tension and $2H$ denotes the total curvature.

NUMERICAL MODEL

To solve the Navier-Stokes equations numerically, the computational domain is covered with a fixed Cartesian grid. The variables are staggered, which means that the velocities are defined at cell faces, whereas the pressure is defined in cell centers.

The body geometry is piecewise linear and cuts through the fixed rectangular grid. Volume apertures (F^b) and edge apertures (A^x, A^y, and A^z) are used to indicate for each cell which part of the cell and cell face respectively is open for fluid and which part is blocked by solid geometry. To track the free surface, the volume-of-fluid function F^s is used, which is 0 if no fluid is present in the cell, 1 if the cell is completely filled with fluid and between 0 and 1 if the cell is partly filled with fluid.

The Navier-Stokes equations are solved in every cell containing fluid. Cell labeling is introduced to distinguish between cells of different characters. First the cells which are completely blocked by geometry are called B(oundary) cells. These cells have volume aperture F^b=0. Then the cells which are empty, but have the possibility of letting fluid flow in are labeled E(mpty). The adjacent cells, containing fluid, are S(urface) cells. The remaining cells are labeled as F(luid) cells. Note that these cells do not

have to be completely filled with fluid. In Figure 1 an example of the labeling is given.

Figure 1: Cell labeling: dark grey denotes solid body, light grey is liquid

Discretisation of the continuity equation

The continuity and Navier-Stokes equations are discretised using the finite volume method. The natural form of the equations when using the finite volume method is the conservative formulation as given in Eq. (1) and (2). In this paper, the discretisation is explained in two dimensions. In most situations, this can be extended to three dimensions in a straightforward manner. In
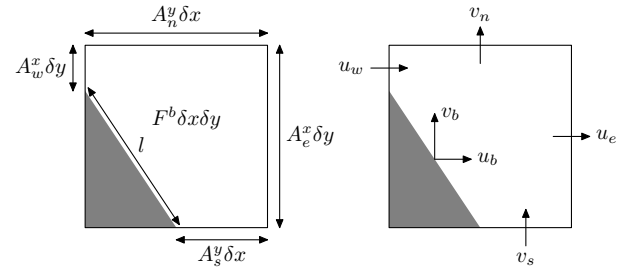

Figure 2: Conservation cell for the continuity equation

Figure 2 a computational cell is shown, which is cut by the body geometry. When applying conservation of mass in this cell, the discretisation results in

$$u_e A_e^x \delta y + v_n A_n^y \delta x - u_w A_w^x \delta y - v_s A_s^y \delta x + u_b(A_e^x - A_w^x)\delta y + v_b(A_n^y - A_s^y)\delta x = 0, \tag{6}$$

where the notation is explained in Figure 2.

Discretisation of the Navier-Stokes equations

For the discretisation of the Navier-Stokes equations, control volumes are defined containing velocities which are defined on cell faces. In the case of uncut cells, the control volume of a velocity simply consists of the right half of the cell left of the velocity and the left half of the cell right of the velocity. In case of cut cells the procedure to define control volumes has been explained in detail in [Gerrits, 2001].

The time derivative in the Navier-Stokes equations is discretised in space using the midpoint rule. This results in

$$\int_V \frac{\partial u}{\partial t} dV \doteq \frac{\partial u_c}{\partial t} F_c^b \delta x_c \delta y. \tag{7}$$

Here, u_c is the central velocity around which the control volume is placed and $F_c^b \delta x_c \delta y$ is the volume of the control volume.

The convective term is discretised directly from the boundary integral which is given by

$$\oint_{\partial V} u \boldsymbol{u} \cdot \boldsymbol{n} dS. \tag{8}$$

Note, that this integral contains two different velocities: the scalar velocity u is advected with the velocity vector $\boldsymbol{u}$. This integral is evaluated along all boundaries of the control volume by multiplying the scalar velocity u with the mass flux through the boundary $\boldsymbol{u} \cdot \boldsymbol{n} dS$. Finally, the convective term discretisation results in a matrix that is skew symmetric, which is also a property of the continuous convective operator [Verstappen, 2003].

The diffusive term, which for the Navier-Stokes equation in x-direction is given by

$$\frac{1}{\rho} \oint_{\partial V} \mu \frac{\partial u}{\partial \boldsymbol{n}} dS, \tag{9}$$

is discretised along all boundaries of the control volume. To ensure stability, the term $\frac{\partial u}{\partial \boldsymbol{n}}$ is discretised in cut-cells as if the cells are uncut. The error introduced this way is small and has no influence in the convection-dominated simulations. The discretisation results in a symmetric matrix which is negative definite.

The pressure term is discretised as a boundary integral, resulting for the Navier-Stokes equation in x-direction in

$$\oint_{\partial V} p n_x dS \doteq (p_e - p_w) A_c^x \delta y. \tag{10}$$

Here, p_e and p_w are the pressure in the eastern and western cell respectively, A_c^x is the edge aperture of the cell face where the central velocity is defined.

The external force is discretised similar to the time derivative, resulting for the x-direction in

$$\int_V F_x dV \doteq F_{x_c} F_c^b \delta x_c \delta y. \tag{11}$$

Here, F_{x_c} is the force at the location of the central velocity.

A detailed explanation of the discretisations described in this section is given in [Gerrits, 2001].

Temporal discretisation

The continuity and Navier-Stokes equations are discretised in time using the forward Euler method. This first order method is accurate enough, because the order of the overall accuracy is already determined by the first order accuracy of the free surface displacement algorithm. Using superscript n for the time level, the temporal discretisation results in

$$M \boldsymbol{u}_h^{n+1} = 0, \tag{12}$$

$$\Omega \frac{\boldsymbol{u}_h^{n+1} - \boldsymbol{u}_h^n}{\delta t} + C(\boldsymbol{u}_h^n) \boldsymbol{u}_h^n = -\frac{1}{\rho}(M^\intercal \boldsymbol{p}_h^{n+1} - \mu D \boldsymbol{u}_h^n) + \boldsymbol{F}_h^n. \tag{13}$$

The continuity equation is discretised at the new time level to ensure a divergence free velocity field. The spatial discretisation is written in matrix notation where M is the divergence operator, Ω contains cell volumes, C contains the convection coefficients (which depend on the velocity vector) and D contains diffusive coefficients.

Solution method

To solve the system of equations, the equations are rearranged to

$$\boldsymbol{u}_h^{n+1} = \tilde{\boldsymbol{u}}_h^n + \delta t \Omega^{-1} \frac{1}{\rho} M^\intercal \boldsymbol{p}_h^{n+1}, \tag{14}$$

where

$$\tilde{\boldsymbol{u}}_h^n = \boldsymbol{u}_h^n - \delta t \Omega^{-1}(C(\boldsymbol{u}_h^n)\boldsymbol{u}_h^n - \frac{\mu}{\rho} D \boldsymbol{u}_h^n - \boldsymbol{F}_h^n). \tag{15}$$

First, an auxiliary vector field $\tilde{\boldsymbol{u}}_h^n$ is calculated using Eq. (15). Next, Eq. (14) is substituted in Eq. (12) which results in a Poisson equation for the pressure. From this equation the pressure is solved using the SOR (Successive Over Relaxation) method where the optimal relaxation parameter is determined during the iterations [Botta, 1985]. Once the pressure field is known, the new velocity field is calculated from $\tilde{\boldsymbol{u}}_h^n$ using the pressure gradient.

Free surface displacement

After the new velocity field has been calculated, the free surface can be displaced. This is done using an adapted version of the volume-of-fluid method first introduced by [Hirt, 1981]. A piecewise constant reconstruction of the free surface is used, where the free surface is displaced by changing the VOF-value in a cell using calculated fluxes through cell faces.

The original VOF method has two main drawbacks. The first is that flotsam and jetsam can appear, which are small droplets disconnecting from the free surface. The other drawback is the gain or loss of water due to rounding of the VOF function. By combining the VOF method with a local height function as introduced in [Gerrits, 2001], these problems do not appear any more. The resulting method is strictly mass conservative.

FREE SURFACE BOUNDARY CONDITIONS

At the free surface, boundary conditions are needed for the pressure and the velocities. The pressure in surface cells is calculated as an interpolation or extrapolation from the pressure in an adjacent fluid cell and the boundary condition at the free surface. The velocities in the neighbourhood of the free surface can be grouped in different classes (see Figure 3). The first class contains

E	E	E	S
S	S	S	F
S	F	F	F

FF, FS, SS: momentum equation

SE: extrapolation

EE: tangential free surface condition

Figure 3: Different characters of velocities near the free surface

the velocities between two F-cells, between two S-cells and between an S- and F-cell. These velocities are determined by solving the momentum equation, so the velocities are called momentum velocities. The second class consists of the velocities between an S- and an E-cell. These velocities are determined using boundary conditions which will be described below. The last class consists of velocities between two E-cells which are sometimes needed to

solve the momentum equation. These are determined using the tangential free surface condition.

SE-velocities

The choice for the method to determine the velocities at the cell faces between surface and empty cells is very important for the robustness and the accuracy of the flow model. Furthermore, this has an influence on the occurrence of numerical spikes in the pressure signal (see Figure 11 where numerical spikes occur). The reason for pressure spikes is that there is not always conservation of mass in a surface (or empty) cell (depending on the boundary conditions). When such a cell becomes a fluid cell, the pressure reacts with a spike to restore mass conservation.

In the following paragraphs two methods will be described for the definition of free surface velocities.

Method 1: conservation of mass in S-cells The first method demands conservation of mass in surface cells. The SE-velocity or velocities at the faces of a surface cell are chosen such that conservation of mass is satisfied in that cell. The advantage of this method is that no spikes will occur in the pressure signal, because conservation of mass is already satisfied if this surface cell changes to a fluid cell. There are two disadvantages. The first one is that this method is not always robust. In the case of Figure 4 the SE-velocity will become very large. If this configuration does not change during a number of time steps, the method will diverge.
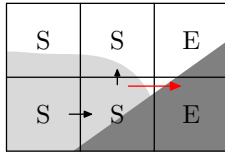

Figure 4: Very large SE velocity when using method 1

The other disadvantage is that the method does not give accurate results in wave simulations. This is shown by the dashed line of Figure 5.

Method 2: extrapolation from direction of fluid In the second method, the SE-velocities are calculated as an extrapolation from the direction of the fluid. Using a linear extrapolation gives very accurate results for steep wave simulations (see Figure 5). But linear extrapolation can lead to instability of the method when the velocity field is not smooth. In that case constant extrapolation is a better choice.

In practice, a method has been chosen which is an engineering mix between the two methods described above. To prevent spikes in the pressure signal, the mass conservation principle has been chosen when a cell changes label from surface cell to fluid cell. In all other cases linear or constant extrapolation is used from the direction of the main body of the fluid, which gives a high accuracy and a very robust method.
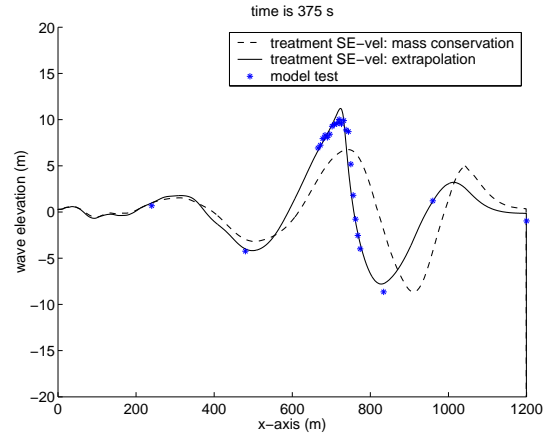

Figure 5: Different methods for free surface velocities in a steep wave simulation

STABILITY

In the case of uncut cells with fixed objects, the stability of the equation containing the time integration term and the convective term is given by the CFL-restriction $\frac{\delta t |u|}{h} \leq 1$. Here, h is the size of the uncut cell. When cut cells are present, this criterion is not changed. This result is not directly straightforward when looking at the equation containing the time derivative and the convective term

$$\frac{\partial \boldsymbol{u}}{\partial t} = -\Omega^{-1} C(\boldsymbol{u}, \boldsymbol{u}_b) \boldsymbol{u} \qquad (16)$$

where $\boldsymbol{u}_b$ is the object velocity. The matrix Ω is a diagonal matrix containing the volumes of the cells, so these entries can become arbitrary small for cut cells. So the elements in the matrix Ω^{-1} can become arbitrary large. But, when estimating the eigenvalues of the convective matrix using Gerschgorin circles by being order $O(\frac{\Omega}{h} u)$, it can be concluded that the same stability criterion is needed as for the uncut-cells case.

When moving objects are present, the story becomes somewhat different. Now, the CFL-criterion does not guarantee stability anymore, because the eigenvalues of $\Omega^{-1} C(\boldsymbol{u}, \boldsymbol{u}_b)$ are of order $O(\Omega^{-1} h \boldsymbol{u}_b)$ which means that they can become arbitrary large. To cancel the effect of Ω a formulation based on a weighted average of the fluid velocity and the boundary velocity should be applied in the cells cut by the moving object. To avoid smearing of the interface in cases where it is not necessary to stabilise the convective term, the following discretisation is used

$$\boldsymbol{u}^{n+1} = \Omega^{n+1}(\Omega^{n+1} + |\Delta\Omega|)^{-1}(\boldsymbol{u}^n + \delta t(\Omega^{n+1})^{-1}$$
$$(-C^n \boldsymbol{u}^n)) + (I - \Omega^{n+1}(\Omega^{n+1} + |\Delta\Omega|)^{-1})\boldsymbol{u}_b^{n+1} \qquad (17)$$

where $\Delta\Omega = \Omega^{n+1} - \Omega^n$ is the difference between Ω's at two different time steps. The factor $\Omega^{n+1}(\Omega^{n+1} + |\Delta\Omega|)^{-1}$ is chosen because then the stabilising term is only used when the body is moving; note that it equals unity for fixed objects. The maximal stabilisation is required when the object is moving normal to its boundary, whereas no stabilisation is needed when the object is moving tangential to its boundary (see Figure 6). A detailed explanation of the stability of the convective terms is given in [Fekken, 2004].
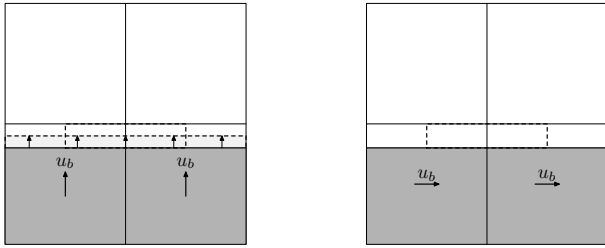
Figure 6: Left: boundary moving normal to itself: maximal stabilisation is required; right: boundary moving tangential to itself: no stabilisation is required

From the diffusive term, also a stability criterion follows with a restriction on the time step. In the case of uncut cells, this criterion is given by $\delta t \leq \frac{h^2}{2\nu}$, where ν denotes kinematic viscosity. Because the diffusive term is discretised as if all cells were uncut ('staircase' approach), the above criterion is also valid in our model.

DAMBREAK SIMULATION

At the Maritime Research Institute Netherlands (MARIN), experiments have been performed for breaking dam flows. These experiments can be seen as a simple model of green water flow on the deck of a ship. The dambreak is a very popular validation case, because the set up is easy, no special in- or outflow conditions are needed. A large tank of 3.22 by 1 by 1 meter is used with an open roof (scale 1:15). The right part of the tank is first closed by a door. Behind the door, 0.55 meter of water is waiting to flow into the tank when the door is opened. At a certain moment, a weight is released which opens the door. In the tank, a box is placed which is a scale model of a container on the deck of a ship.
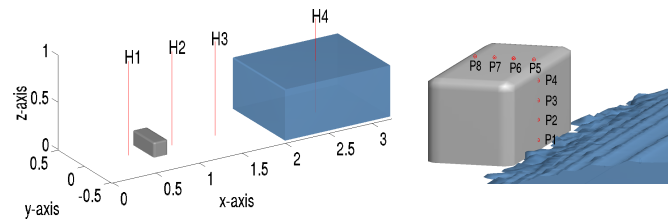

Figure 7: Measurement positions for water heights and pressures in the dambreak experiment

During the experiment, measurements have been performed of water heights, pressures and forces. In Figure 7, the positions of the measured water heights and pressures are shown. In the tank, four vertical wave probes have been used. One in the reservoir and the other three in the tank. The box was covered by eight pressure pick-ups, four on the front of the box and four on the top. The forces on the box were also measured. To determine the velocity of the water when entering the tank, a horizontal wave probe is used near the side wall of the tank.

As starting configuration of the simulation with COMFLOW, the water in the right part of the domain is at rest. When the simulation is started, the water starts to flow into the empty tank due to gravity. In Figure 8 two snapshots of the early stages of

the simulation are shown together with images of the video of the experiment (at the same moments in time). The smaller pictures
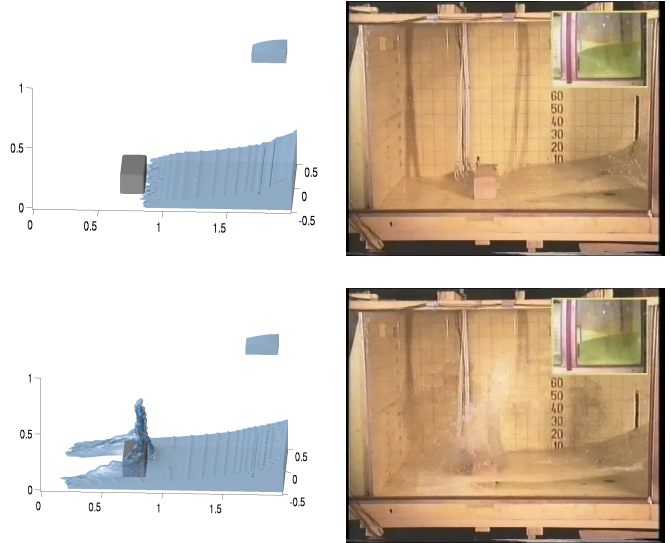

Figure 8: Snapshots of a dambreak simulation with a box in the flow compared with experiment at time 0.4 and 0.56 seconds

inside the snapshots show the water in the reservoir. There is a very large agreement between the simulation and experiment. The moment in time when the water is first hitting the box is the same. The shape of the free surface, bending a bit forwards in the second picture, is seen in both experiment and simulation. In the simulation, the free surface has some ripples, and these are due to the computational grid.
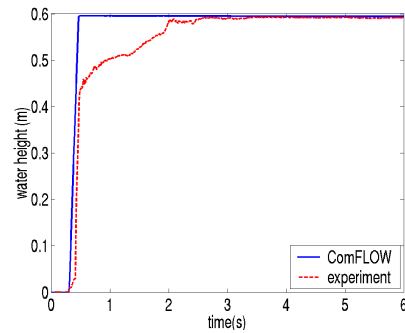

Figure 9: Horizontal wave probe along the side of the tank

In Figure 9 the time history of the horizontal wave probe is shown, compared with the simulation. The first stage of the simulation compares very well with the experiment, the velocity with which the water is flowing into the tank is predicted very well. By the time the water hits the box, there is a difference between the experiment and the simulation. In the experiment, the water is slowed down, the wave probe is totally covered by water only after 2 seconds. In the simulation this is the case after 0.5 seconds. When looking at the movie of simulation and experiment, this difference is not present, suggesting an inconsistency in the wave probe measurements. The flow reaches the end wall at the same time in simulation and experiment. So the appearing difference in Figure 9 is not a real difference between simulation and

experiment.

In Figure 10, the water height at two locations is shown: in the reservoir, and in the tank just in front of the box. The agreement in both pictures is very good until the water has returned from the back wall (after about 1.8 seconds). After that some differences occur, but the global behaviour is still the same. When the water has returned from the wall, the water height at probe H2 is largest. The water flows back to the reservoir, where it turns over again at about 4 seconds. The moment that this second wave meets the wave probe at H2 again is almost exactly the same in simulation and experiment.
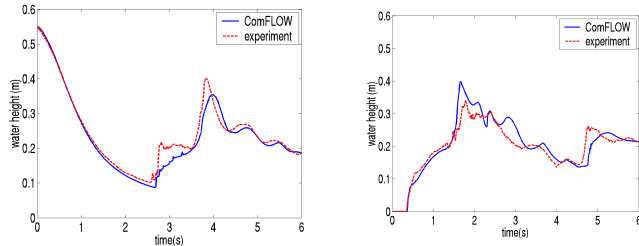

Figure 10: Vertical water heights in the reservoir H4 (left) and the tank H2 (right)
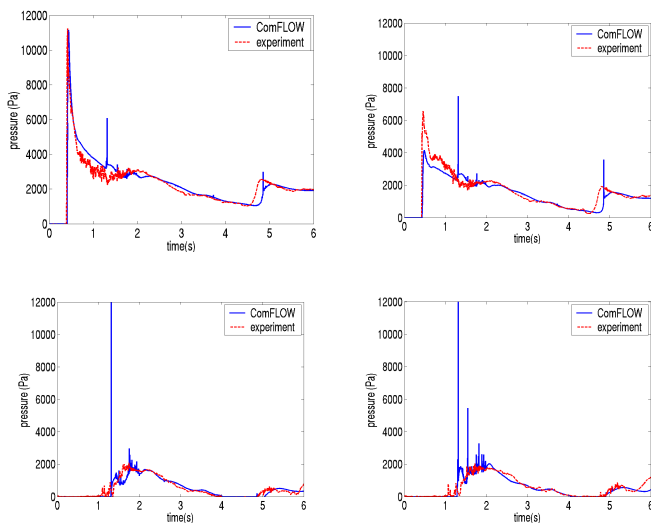

Figure 11: Pressure time histories of P1 (upper left), P3 (upper right), P5 (lower left), and P7 (lower right)

The moment the wave hits the box is perfectly captured by the simulation as can be seen from Figure 11. Here the pressure at point P1 and P3 at the front of the box and at the top of the box, P5 and P7 (see Figure 7), are shown. The magnitude of the impact pressure is the same for simulation and experiment at pressure point P1 (the lowest on the box), but is underpredicted by the simulation at point P3. The moment the return wave hits the box again (at about 4.7 seconds) is again visible in the graphs. In the bottom graphs of Figure 11, where the time history of pressure transducers at the top op the box are shown, a clear difference occurs between simulation and experiment. After about 1.3 seconds, there is a wiggle in the simulation with a duration of 0.5 seconds, which is not present in the experiment. Before this point, the water hits the top of the box when the wave

coming back from the wall is overturning. This difference is a real difference which cannot be explained properly at the moment.

Several spikes appear in the pressure signals, which are spikes in all the graphs at the same moment. These spikes occur, because some water enters an empty cell which is completely surrounded by cells with fluid. Then, this empty cell changes to a fluid cell in one time step without being a surface cell in between. This change in label results in a pressure spike over the whole pressure field.

The results of the dambreak simulation are in good agreement with the experiment. The global behaviour of the fluid is the same and the impact peak of the pressure agrees well, especially at the lowest part of the box.

WATER ENTRY AND EXIT

In this section, validation results of water entry and exit of two-dimensional objects are presented. The simulations have been carried out in two dimensions. The objects are moving according to a constant prescribed motion.

Figure 12 presents free surface profiles for the entry of two wedges. The wedges have deadrise angles of 30 and 45 degrees, respectively. The simulation results have been compared with photographs of experiments by Greenhow [Greenhow, 1983]. The
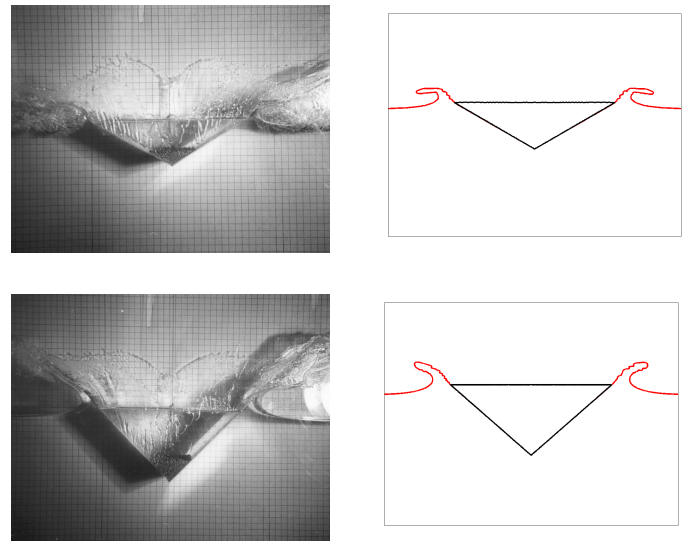

Figure 12: Snapshots of wedge entry with deadrise angles 30 degrees (up) and 45 degrees (down)

simulations have been performed on a grid of 300x280 computational cells. The visual comparison between the experiments and the simulations is very good. The jets which are formed aside of the wedge are created by COMFLOW to a certain extent, but the small details of the jets and the spray are not reproduced, mainly due to the limited number of grid cells.

A visual comparison of the free surface development of cylinder entry is presented in Figure 13. The simulation has been performed on a grid of 400x400 points. The same can be concluded for the cylinder as for the wedges: the details of the spray are not reproduced by COMFLOW.

The total hydrodynamic force on the cylinder during the first stage of the impact has been calculated and compared with ex-
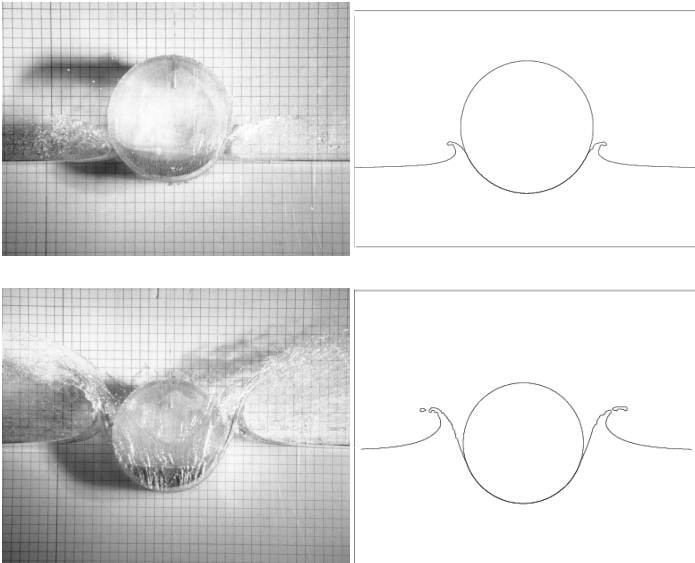
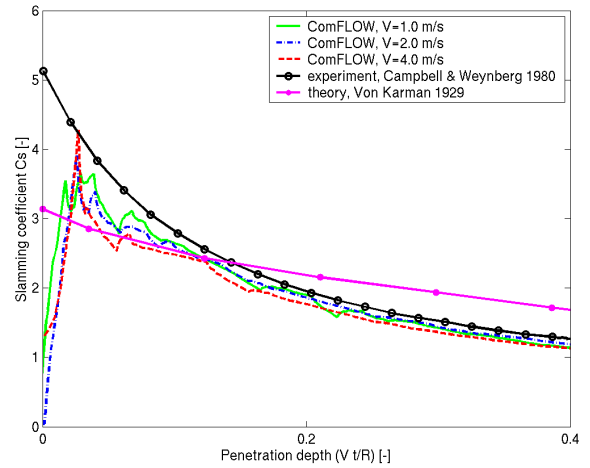Figure 13: Snapshots of the water entry of a circular cylinder

Figure 14: Slamming coefficient of the entry of a circular cylinder compared to the experiments of Campbell & Weynberg and the theory of Von Karman
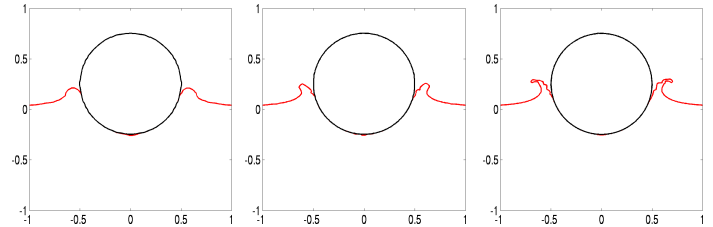

Figure 15: Effect of grid refinement on the jets formed during water entry of a circular cylinder: from left to right 100x100, 200x200 and 400x400 grid cells

perimental results of Campbell and Weynberg [Campbell, 1980], also reported in [Battistin, 2003]. In Figure 14 the slamming coefficients of the cylinder entry with different entry velocities have been plotted versus the nondimensional penetration depth. The slamming coefficient is given by $C_s = F/\rho R V^2$ with F the total vertical hydrodynamic force, R the radius of the circular cylinder and V the entry velocity. Besides the experimental result of Campbell and Weynberg, also the theory of Von Karman (1929), reported by Faltinsen [Faltinsen, 1990], has been included. This theory is based on potential theory. For the very initial stage of the entry of a circular cylinder, the vertical hydrodynamic slamming force can be estimated by

$$F = V\rho\frac{\pi}{2}(2VR - 2V^2t),\qquad(18)$$

where t denotes time with $t = 0$ at the moment of first impact. The comparison between the experiments of Campbell and Weynberg and the simulations is reasonable. It can be seen that the initial impact is a bit underpredicted by ComFLOW for all entry velocities. The initial impact is more in agreement with the theory of Von Karman. In a later stage, the results are in good agreement with the experiments of Campbell and Weynberg. The results of ComFLOW are almost similar for different entry velocities, which confirms near perfect scaling with V^2.

To study the convergence of the method under grid refinement, the circular cylinder entry simulations have been run with different grids also. The results are presented in Figure 15. It can be seen that the coarseness of the grid has a very large influence on the formation of the jets aside the cylinder. A very fine grid is needed to capture the jets. However, the formation of the jets does not have a large influence on the total hydrodynamic force, because of the almost zero pressures inside the jets [Battistin, 2003].

In Figure 16, snapshots of simulations of cylinder exit are compared with photographs of experiments [Greenhow, 1983]. The Froude number, defined by $Fr = \frac{V^2}{Rg}$, is taken 0.41. The simulation has been performed on a grid of 300x280 points. The visual comparison between simulation and experiment is very

good. The free surface development is well resolved by ComFLOW, also the very thin layer of fluid around the cylinder is present.

CONCLUSIONS

In this paper, a numerical method is described for the prediction of local impact loads on floating structures. The method is based on a cut-cell approach on a fixed Cartesian grid, and is stable even when very small cells appear. For the displacement of the free surface, an improved VOF method is used, which results in full mass conservation. The determination of the free surface boundary conditions have shown to have a large influence on the accuracy of wave simulations. To improve this further, the method will be extended to a two-phase fluid flow model, in which these boundary conditions will not be needed any more.

The method has been validated using two kinds of simulations. The first simulation is a dambreak simulation with a box in the flow. Time series of pressure and water height have been compared with measurements from MARIN. The results are satisfying, especially when considering that the flow is very violent. The global behaviour of the fluid is very much the same. The second kind of validation consists of water entry and exit of wedges and cylinders. The development of the free surface has been com-
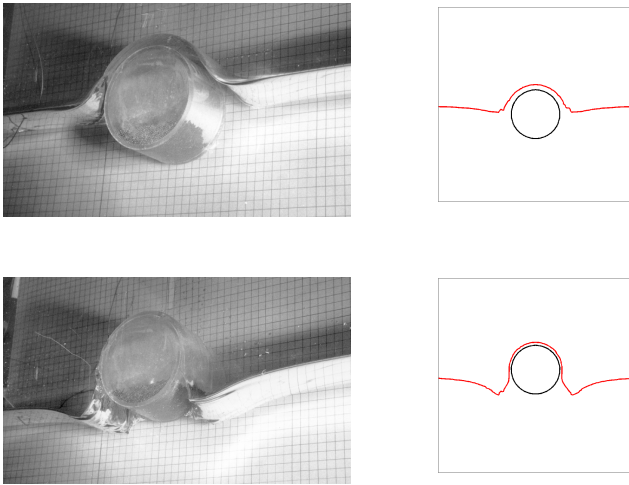
Figure 16: Snapshots of cylinder exit at t=0.9 seconds and t=1.06 seconds, with exit velocity V=1 m/s

pared with experimental results, where a good comparison has been found. Also the jets appearing at the sides of the wedges and cylinders are resolved by ComFLOW, although the details of the spray are not reproduced. Using a finer grid gives a large improvement for the reproduction of the jets. The hydrodynamic forces during the impact of a cylinder entering the water have been compared with experiments and theory, which show a rather good agreement.

The next step in the validation of the method will be to simulate green water due to large waves which flow over the deck of a floating vessel. In the coming years, the method will be extended with a coupling to an outer domain where waves are generated using a much cheaper diffraction code. In this way, the ComFLOW domain can be limited to the close surroundings of the places of impact.

ACKNOWLEDGMENT

REFERENCES

Battistin, D., Iafrati, A., "Hydrodynamic loads during water entry of two-dimensional and axisymmetric bodies", *J. Fluids Struc.*, **17**, 643-664, 2003.

Botta, E.F.F., Ellenbroek, M.H.M., "A Modified SOR Method for the Poisson Equation in Unsteady Free-Surface Flow Calculations", *J. Comp. Phys.*, **60**, 119-134, 1985.

Fekken, G., Buchner, B., Veldman, A.E.P., "Simulation of green-water loading using the Navier-Stokes equations", J. Piquet, editor, *Proc. 7th Int. Conf. on Numerical Ship Hydrodynamics*, 6.3-1-6.3-12, Nantes, 1999.

Campbell, I.M.C., Weynberg, P.A., "Measurement of parameters affecting slamming", *Report No. 440, Wolfson Unit of Marine Technology, Tech. Rep. Centre No. TO-R-8042*, Southampton, 1980.

Faltinsen, O.M., *Sea loads on ships and offshore structures*, Cambridge University Press, Cambridge, 1990.

Fekken, G., *Numerical Simulation of Free-Surface Flow with Moving Rigid Bodies*, PhD thesis, University of Groningen, March 2004, URL: http://www.ub.rug.nl/eldoc/dis/science/g.fekken.

Greenhow, M., Lin, W.-M. "Nonlinear free surface effects: experiments and theory", *Rep. No 83-19, Department of Ocean Engineering, MIT*, Cambridge, Mass, 1983.

Gerrits, J., *Dynamics of Liquid-Filled Spacecraft*, PhD thesis, University of Groningen, December 2001, URL: http://www.ub.rug.nl/eldoc/dis/science/j.gerrits.

Hirt, C.R., Nichols, B.D. "Volume of fluid (VOF) method for the dynamics of free boundaries", *J. Comp. Phys.*, **39**, 201-225, 1981.

Loots, G.E., Hillen, B., Veldman, A.E.P., "The role of hemodynamics in the development of the outflow tract of the heart", *J. Eng. Math.*, **45**, 91-104, 2003.

Verstappen, R.W.C.P., Veldman, A.E.P., "Symmetry-preserving discretization of turbulent flow", *J. Comp. Phys*, **187**, 343-368, 2003.